Dynamic functional contribution of the water channel AQP5 to the water permeability of peripheral lens fiber cells

Rosica S. Petrova[1], Kevin F. Webb[3], Ehsan Vaghefi[2], Kerry Walker[1], Kevin L. Schey[4], Paul J. Donaldson[1,2*]

[1]Department of Physiology, School of Medical Sciences, and [2]School of Optometry & Vision Sciences, New Zealand National Eye Centre, University of Auckland, Auckland, New Zealand; [3]Optics & Photonics Research Group, School of Electrical & Electronic Engineering University of Nottingham, Nottingham, UK, and [4]Mass Spectrometry Research Centre, Vanderbilt University, Nashville, TN, USA

Running title: AQP5 insertion increases lens fiber cells water permeability

Corresponding Author*:

Paul J Donaldson, PhD
Department of Physiology
School of Medical Sciences
University of Auckland
Email: p.donaldson@auckland.ac.nz
Ph: +64 9 9233174

Key words: lens**,** aquaporin (AQP), water permeability, fiber cell membrane vesicles, hydrostatic pressure of the lens

ABSTRACT.

Although the functionality of the lens water channels, AQP1 (epithelium) and AQP0 (fiber cells), are well established less is known about the role of AQP5 in the lens. Since in other tissues AQP5 functions as a regulated water channel with a water permeability (P_{H2O}) some 20x higher than AQP0, AQP5 could function to modulate P_{H2O} in lens fiber cells. To test this possibility a fluorescence dye dilution assay was used to calculate the relative P_{H2O} of epithelial cells and fiber membrane vesicles isolated from either the mouse or rat lens, in the absence and presence of $HgCl_2$ - an inhibitor of AQP1 and AQP5. Immunolabeling of lens sections and fiber membrane vesicles from mouse and rat lenses revealed differences in the subcellular distributions of AQP5 in the outer cortex between species - with AQP5 being predominantly membranous in the mouse, but predominantly cytoplasmic in the rat. In contrast, AQP0 labelling was always membranous in both species. This species-specific heterogeneity in AQP5 membrane localisation was mirrored in measurements of P_{H2O}, with only fiber membrane vesicles isolated from the mouse lens exhibiting a significant Hg^{2+}-sensitive contribution to P_{H2O}. When rat lenses were first organ cultured, immunolabeling revealed an insertion of AQP5 into cortical fiber cells, and a significant increase in Hg^{2+}-sensitive P_{H2O} was detected in membrane vesicles. Our results show that AQP5 forms functional water channels in the rodent lens, and suggests that dynamic membrane insertion of AQP5 may regulate water fluxes in the lens by modulating P_{H2O} in the outer cortex.

INTRODUCTION

The aquaporin (AQP) family of water channels mediate the passive diffusion of water across cell membranes and, as such, play major roles in many physiological and pathological processes (32). Thirteen AQP isoforms have been identified in humans, and ongoing research has shown that differences in water permeability, transcriptional regulation, post-translational modification, protein stability and polarized membrane distribution between the different AQP isoforms accounts for the functional differences in water permeability observed at the cellular level in different tissues (1, 9, 25). In the ocular lens, AQPs are considered essential to the lens internal microcirculation system that generates circulating ionic and fluid fluxes which, in the absence of a blood supply, deliver nutrients to and remove waste products from the lens centre faster than would occur by passive diffusion alone (39, 40).

The microcirculation system and specialized architecture of the lens maintain its transparency and homeostasis. The lens anterior surface is covered with a single layer of epithelial cells while the bulk of the lens is formed of highly elongated fiber cells organized in concentric growth rings (4). The lens continues to grow throughout life by the addition of new fiber cells formed by the terminal differentiation of epithelial cells localized at the lens equator. In this way, the older and organelle-free mature fiber cells are encapsulated into the deeper core of the lens, whereas the youngest and metabolically-active differentiating fiber cells are found in the peripheral outer cortex of the lens (38, 41). Superimposed upon this gradient of lens development, differentiation and growth are spatial differences in the expression and post-translational modification of at least three AQP isoforms. AQP0 (19), AQP1 (49) and most recently AQP5 expression in the lens has been confirmed in multiple species (20, 34), and changes in the expression patterns during mouse lens development and growth have been mapped (44, 49).

AQP1 is abundantly expressed in a variety of tissues (2), and in the eye is found in the corneal endothelium, amacrine and glial cells of the retina, and in the lens epithelium (8, 24, 31). During development, AQP1 is firstly expressed in lens epithelial cells at embryonic day 17 in the mouse lens. AQP1 expression progressively increases during postnatal development, which coincides with an increase in the size of the lens (50). This increased expression of AQP1 translates into an increase in the mercury-sensitive water permeability of isolated lens epithelial cells (10, 50). Deletion of AQP1 in the lens epithelium resulted in an approximately three-fold reduction of the water permeability of AQP1 knock-out mouse lenses (46). Although lack of AQP1 expression did not affect lens morphology and transparency, it was found that incubation of lenses from AQP1 knockout mice in high glucose solutions resulted in accelerated loss of lens transparency relative to that seen in wild type lenses. Therefore, AQP1 is required to maintain the transparency of the lens, especially following exposure to stress conditions such as hyperglycemia and osmotic imbalance.

AQP0, previously known as major intrinsic protein 26 (MIP26), is a highly abundant protein which constitutes over 60% of the total membrane protein content of the lens (7). AQP0 was thought to be exclusively expressed in in lens fiber cells, although recent reports show weak immunoreactivity in bipolar, amacrine and ganglion cells of the retina (11, 23). AQP0 is a low-conductance water channel, with water permeability some 30- and 20-fold lower than AQP1 and AQP5 respectively (10, 42, 57). AQP0 can double its permeability in mildly acidic environments (48). Unlike AQP1 and AQP5, AQP0 is not sensitive to inhibition by mercury (42), due to the absence of a cysteine residue contained within the water pore which, in other AQP isoforms, renders the water channel sensitive to mercurial inhibition (33, 47). As the lens grows and ages, AQP0 undergoes differentiation-dependent post-translational modifications to its *C*-terminal domain, including phosphorylation, truncation, glycation and

deamidation (3). While the effect of glycation and deamidation on AQP0 water permeability is unclear, the most abundant modifications, phosphorylation and truncation, are thought to alter the regulation of its water permeability. Several sites of phosphorylation have been identified (45), while extensive *C*-terminal truncation has been well characterized in the core of the lens (19, 54). Phosphorylation of AQP0 at Serine 235, the most abundant phosphorylation site, occurs via PKA and is mediated by AKAP2 (16). The phosphorylation of the *C*-terminal tail has been shown to disrupt calmodulin binding (45), and therefore changes the regulation of AQP0 activity in the presence of elevated Ca^{2+}. Structurally, AQP0 have been shown to exists in two conformations suggesting a change of AQP0 function from a water pore in the periphery to an adhesion protein in the core of the lens through its identification within 11-13 nm "thin lens junctions" (17, 18, 21).

AQP5 is a water channel recently identified in epithelial and fiber cells of the ocular lens at the gene (43, 55) and protein (5, 54) levels. Most recently, its expression was verified not only in our laboratory (20) but also by other researchers (34). Interestingly, immunohistochemical mapping of AQP5 distribution across the lens radius (20), revealed a differentiation-dependent change in the sub-cellular localization of AQP5 from a cytoplasmic to membranous labeling pattern with fiber cell differentiation, and therefore radial position within the lens. Furthermore, the labeling pattern observed for AQP5 in the outer cortex of the lens was very different to that observed for AQP0, which is always membranous in the young, differentiating fiber cells present in this region (19). These differences in membrane localization of AQP5 relative to AQP0 raises questions about the relative functional roles of the two AQPs in the different regions of the lens, especially since AQP5 has a ~20 fold higher water permeability than AQP0 (57), although AQP0 is 100 times more abundant than AQP5 (5).

To determine whether AQP5 contributes to the water permeability of peripheral lens fiber cells, we have in this study employed a fluorescence dye-dilution assay that utilizes fiber cell membrane vesicles isolated from the outer cortex of either the mouse or rat lens. In parallel we show species-specific differences in AQP5 membrane labeling levels, and hence differences in the potential contribution of AQP5 to overall water permeability. To distinguish the relative contributions of AQP5 and AQP0 to overall water permeability, vesicles from both species were incubated in the absence or presence of mercury ($HgCl_2$), which blocks AQP5, but not AQP0 water channels. Our results suggest not only that AQP5 contributes to the water permeability of cortical fiber cells, but also that the water permeability in this region can be dynamically upregulated by the insertion of AQP5 from a cytoplasmic pool into the membranes of differentiating fiber cells.

MATERIALS AND METHODS

Reagents

An affinity-purified anti-AQP5 antibody directed against the final 17 amino acids (rat sequence) of the C-terminus of the protein, was obtained from Millipore (Billerica, MA, Cat#: AB15858). Affinity-purified anti-AQP0, directed against the final 17 amino acids (human sequence) of the C-terminus of the protein, was obtained from Alpha Diagnostic International, Inc. (San Antonio, TX, Cat#: AQP01-A). Secondary antibodies (goat anti-rabbit-Alexa 488), fluorophore-conjugated wheat germ agglutinin (WGA-Alexa Fluor 594) for labelling of cell membranes, and calcein acetoxymethyl ester (calcein-AM) used for fluorescent loading of epithelial cells and fiber cell membrane vesicles were each obtained from Thermofisher Scientific (Waltham, MA, USA). DAPI, obtained from Sigma Aldrich (St Louis, MO), was used for fluorescent labeling of cell nuclei. Phosphate buffered saline (PBS, pH 7.4) was prepared fresh from PBS tablets. Unless otherwise stated all other chemicals were from Sigma Aldrich.

Collection and preparation of lenses

Adult mouse and rat lenses were removed from C57BL/6 mice or Wistar rats immediately following death, using procedures in accordance with the ARVO Statement for the Use of Animals in Ophthalmic and Vision Research, which were approved by the University of Auckland Animal Ethics Committee (#001303). Following extraction, lenses were either immediately placed in fixative and subsequently processed for immunohistochemistry, placed in warm PBS prior to preparation of isolated epithelial cells or fiber cell vesicles, or prepared for organ culturing from 2 to 17 hours in Artificial Aqueous Humour (AAH: containing 125 mM NaCl, 0.5 mM $MgCl_2$, 4.5 mM KCl, 10 mM $NaHCO_3$, 2 mM $CaCl_2$, 5 mM glucose, 10 mM sucrose, 10 mM HEPES, pH 7.4, 300 $mOsmL^{-1}$). At the end of the incubation period,

organ cultured lenses were either immediately fixed in 0.75% paraformaldehyde and processed for immunohistochemistry, or used to isolate fiber cell vesicles.

Isolation of lens epithelial cells and fiber cell membrane vesicles

Immediately following extraction from the eye, or after organ culture in AAH, a pair of sharpened forceps was used to separate and remove the lens capsule and adherent epithelial cells from the underlying fiber cell mass. Forceps were then used to peel off small clumps of differentiating fiber cells from the outer cortical fiber cell mass. The lens capsule was incubated in collagenase dissociation buffer (150 mM Na-gluconate, 4.7 mM KCl, 5 mM glucose, 5 mM HEPES, 0.125% Type IV collagenase, pH 7.4) for 30 minutes at 37 $^{\circ}$C to isolate lens epithelial cells. After the first 15 minutes of incubation, 4 µM calcein-AM was added to the dissociation buffer to label dissociated epithelial cells with fluorescent calcein during the remaining 15 minutes of the dissociation incubation period. Epithelial cells were pelleted at 150 g for 3-5 minutes using a bench-top microcentrifuge and washed twice with 300 $mOsmL^{-1}$ isotonic saline (139 mM NaCl, 4.7 mM KCl, 1 mM $MgCl_2$, 5 mM glucose, 5 mM HEPES, pH 7.4, 300 $mOsmL^{-1}$). To form fiber cell membrane vesicles, clumps of differentiating fiber cells were isolated from the outer cortex of the lens with forceps and transferred to isotonic saline which contained 5 mM $CaCl_2$. Clumps of fiber cells were incubated for 30 minutes at room temperature (20 ^{o}C), which induced spontaneous formation of vesicles (51). To load these fiber cell-derived membrane vesicles with fluorophore, 6 µM calcein-AM was added to the Ca^{2+}-containing isotonic saline for the duration of the 30 minutes incubation time. Membrane vesicles were then pelleted at 150 g for 3-5 minutes and washed twice in Ca^{2+}-free isotonic saline for immediate use in the fluorescence dye-dilution assay.

Immunolabeling of lens sections and fiber cell membrane vesicles

Lenses, either immediately post-extraction from the eye, or after organ culture, were fixed in 0.75% paraformaldehyde at room temperature for 24 hours, and prepared for cryosectioning using previously-published protocols (28). For sectioning, whole lenses were mounted encased in optimal cutting temperature (OCT) compound (Tissue-Tek; Sakura Finetek, Zoeterwoude, The Netherlands), and snap frozen in liquid nitrogen for 15-20 seconds. Lenses were cryo-sectioned at –19 °C using a cryostat (CM3050, Leica Microsystems, Germany), and 14 μm-thick equatorial cryosections were transferred onto plain microscope slides. Isolated fiber membrane vesicles were plated for immunolabeling experiments on plain microscope glass slides, before being fixed for 30 minutes in 2% paraformaldehyde. Both lens sections and fiber-derived membrane vesicles were subjected to the same established immunohistochemistry protocols (19). Briefly, fixed lens sections or fiber membrane vesicles were first incubated in blocking solution (3% bovine serum albumin, 3% normal goat serum in PBS pH 7.4) for 1 hour at room temperature. After washing in PBS pH 7.4, samples were incubated in primary antibody in blocking solution (1:100) overnight at 4 °C. Samples were washed in PBS pH 7.4 and incubated for 1.5 hours, at room temperature in the dark with fluorescent secondary antibodies in blocking solution (1:200), or contained 0.125μg/ml DAPI to stain cell nuclei of lens sections. Where necessary, sections were then incubated with WGA-Alexa Fluor 594 in PBS pH 7.4 (1:100) for 1 hour (room temperature) to label cell membranes. Lens sections and membrane vesicles were cover-slipped using VectaShield HardSet™ anti-fade mounting medium (Vector Laboratories, Burlingame, CA). Immunofluorescent images were acquired using a laser scanning confocal microscope (Olympus FV1000, Tokyo, Japan) equipped with FluoView 2.0b software. For presentation, labeling patterns were pseudo-colored and combined using Adobe Photoshop CS6 (Adobe Systems Inc., San Jose, CA).

Fluorescence dye-dilution assay for water permeability

Calcein-AM-loaded epithelial cells or fiber cell membrane vesicles were attached to the bottom of a custom-made recording chamber using Cell-Tak^{TM} adhesive agent (Corning, Two Oak, Bedford, USA) for 30 minutes at room temperature. To remove loosely-attached cells or vesicles, 300 $mOsmL^{-1}$ isotonic saline was washed through the recording chamber for 5 minutes using a gravity-fed perfusion system which allowed the composition of the bath to be completely changed with a time constant of 2 seconds. The chamber was mounted on a Nikon Eclipse TE 300 inverted epifluorescence microscope, equipped with a 40x CFI Plan Fluor NA 0.75 objective and a filter set (Nikon, B-2A) that matched the excitation and emission spectra of calcein-AM. Differential Interference Contrast (DIC) and epifluorescence images were collected using an electron-multiplying CCD camera (Cascade II 512B emCCD, Photometrics, Tucson, USA), suitable for imaging in low-light applications with rapid frame rates. Imaging protocols consisted of collecting an initial DIC image of epithelial cells or fiber cell membrane vesicles to allow accurate measurement of their initial cross sectional area in isotonic saline. Subsequently, a series of fluorescence images were collected at 2Hz to record the time-course of change in fluorescence intensity in response to a 390 $mOsmL^{-1}$ hypertonic challenge, induced by switching incoming bathing solution from isotonic to hypertonic saline, which contained 185 mM NaCl (Figure 1A). Images were acquired using Imaging Workbench 5.2 (Indec BioSystems, Los Altos, USA). Regions of interest were created within the boundaries of individual epithelial cells or fiber-derived vesicle, thereby enabling changes in fluorescence intensity in response to alterations in the volume of an epithelial cell or vesicle to be captured in real time (Figure 1B). Hypertonic challenge was performed either in the absence or presence of 300 μM $HgCl_2$, an irreversible inhibitor of AQP5 and AQP1 channels (33, 47), but not AQP0 water channels (42). The effect of mercury was examined by a 5 minute pre-incubation of lens epithelial cells or fiber cell membrane

vesicles in isotonic saline containing 300 μM $HgCl_2$, before applying identical hypertonic challenge in the presence of 300 μM $HgCl_2$

Calculation of water permeability.

The water permeability of epithelial cells and fiber cell-derived membrane vesicles have been determined by modifying the equation adopted from a paper published by Varadaraj et al. in 1999 (51)

$$\boldsymbol{P_{H2O}=\frac{1}{Sm}\frac{C_{H2O}}{C_i(0)-C_0}\frac{dV_i(0)}{dt}} \quad (1)$$

Equation 1 is based on the assumption that water flows across a cell membrane in response to the gradient of osmolarity, $\boldsymbol{\frac{C_{H2O}}{C_i(0)-C_0}}$ established across the membrane, at a rate determined by the surface area, S_m, and rate of change of volume, $\boldsymbol{\frac{dV_i(0)}{dt}}$. Since in our method we used a fluorescent tracer to follow the change in volume, instead of monitoring the change in cross sectional area, we modified the Equation 1 to fit our assay system which measures the time course of the rate in change of fluorescence intensity in response to hypertonic challenge. This response is given by Equation 2

$$\boldsymbol{P_{H2O}=\frac{1}{Sm}\frac{C_{H2O}}{C_i(0)-C_0}\frac{dF_i(0)}{dt}} \quad (2)$$

To calculate the water permeability the membrane surface area ($\boldsymbol{S_m}$) was measured using DIC images that captured the initial morphology of the epithelial cell or fiber cell membrane vesicles showing near perfect spherical shape for these objects (Figure 1A), and then calculated using Equation 3.

$$\boldsymbol{S_m= 4\pi r^2} \quad (3)$$

where the radius (r, μm) was obtained using the cross sectional area (A) calculated by tracing the pixels within the defined region of interest using Image J software, (Equation 4).

$$\boldsymbol{r} = \sqrt{\frac{\boldsymbol{A}}{\boldsymbol{\pi}}} \quad (4)$$

Imaging Workbench 5.2 software was used off-line to quantify the change in fluorescence intensity in response to hypertonic challenge within individual calcein-AM loaded epithelial cells or fiber membrane vesicles. Correction for photo-bleaching was applied by normalizing data against a monoexponential function fitted to the initial, pre-challenge, region of the timecourse using Clampfit 9.2 (Molecular Devices, Sunnyville, CA) to produce a bleach-corrected timecourse showing the change in fluorescence intensity caused in response to hyperosmotic challenge (Figure 1B). A monoexponential of the form $\boldsymbol{y = Ae^{-\tau t} + C}$ was fitted to the fluorescence response to challenge (Figure 1C), and the time constant (τ) extracted to quantify the rate of change of fluorescence using the best fit values for the initial and final fluorescence F1 and F2 (Equation 5):

$$\frac{\boldsymbol{dF_i(0)}}{\boldsymbol{dt}} = \frac{\boldsymbol{F2-F1}}{\boldsymbol{\tau}} \quad (5)$$

The rate of change in fluorescence intensity (Equation 5) along with the external osmotic gradient and initial resting area were fitted into Equation 2 to calculate the relative water permeability of epithelial cells and fiber cell membrane vesicles expressed in arbitrary units (AU), where $C_{H2O} \approx 55M$ is the concentration of water and $C_{i(0)}$ = 300 mOsmL-1 is the initial bathing solution, assumed to be equal to the initial intracellular osmolarity, and C_0 = 390 $mOsmL^{-1}$. We applied this approach for calculation of the water permeability of epithelial cells and membrane vesicles since it has been shown that using mono-exponential fits of

normalized fluorescence data is more accurate and mathematically stable, for calculation of a decay rate (30, 56), whereas usage of multi-exponential and parameterised interpretation of fluorescent decays is inaccurate (35, 36, 56). Following this rationale we have chosen to normalize our dataset of change of fluorescence time course and use arbitrary units (AU) for our rate calculations.

Statistical analysis

To evaluate the water permeability of lens epithelial cells or fiber cell membrane vesicles, data were obtained from at least 3 animals performed through at least 3 separate experiments. Mean data of experiments are given ± standard error of the mean (SEM). Statistical significance was tested with the Mann-Whitney U test, using GraphPad Prism (La Jolla, California, USA). * indicates statistically significant differences at the $\alpha=0.05$ level..

RESULTS

Species differences in the membrane localization of AQP5 in rodent lenses and fiber-cell-derived membrane vesicles

In previous studies, we have used immunohistochemistry to map the distribution of AQP0 in the rat lens (19), and AQP0 and AQP5 in the mouse lens (20, 44). In these previous studies we, noted subtle species differences in the distribution of AQP5 in the outer cortex. In the present study, we applied our immunohistochemistry mapping approach to axial sections to examine more closely how these differences in distribution of AQP5 in the adult mouse and rat lens manifest as fiber cells proceed through the different stages of differentiation and elongation to reach the anterior and posterior poles of the lens (Figure 2). We confirmed our previous observation, that in differentiating fiber cells AQP5 is predominately cytoplasmic in peripheral fiber cells, but undergoes a distinctive translocation to the membranes of elongating fiber cells at distinct stages of fiber cell differentiation. In the current study, we also show that the radial location of this transition is species-dependent. In the mouse lens, the pool of cytoplasmic AQP5 labelling was confined to a narrow, superficial zone located to the lens modiolus at the equator (Figure 2, Region 1B). Either side of the modiolus region, AQP5 is inserted into the membranes of elongating fiber cells (Figure 2A), with AQP5 labeling becoming strongly associated with the membranes of fiber cells that reach both the anterior (Figure 2, Region 2B) and posterior poles of the lens (Figure 2, Region 3B). In contrast, in the rat lens, AQP5 exhibited predominately cytoplasmic labeling throughout the entire equatorial region (Figure 2, Region 1C), remaining cytoplasmic in differentiating fiber cells as they elongated to reach both the anterior (Figure 2, Region 2C) and posterior (Figure 2, Region 3C) poles of the lens.

These observed differences of expression of AQP5 in the axial direction in rodent lenses reinforced earlier descriptions along the continuum of differentiation in the equatorial orientation (Figure 3), (20). Mouse AQP5 labeling was cytoplasmic in peripheral fiber cells as they differentiated from epithelial into fiber cells at the equator of the lens (Figure 3C). At deeper locations, associated with later stages of fiber cell differentiation, AQP5 labeling abruptly became associated with the plasma membrane, with this membranous labeling then being retained in the rest of the outer cortex of the mouse lens (Figure 3E). In contrast, in the rat lens, AQP5 labeling remained predominately cytoplasmic in differentiating fiber cells throughout the outer cortex (Figure 3J&I). AQP0, on the other hand, at these location, was always membranous in both the mouse (Figure 3B&D) and rat lenses (Figure 3F&H). Based on these observed regional differences in the membrane distribution of AQP5 and AQP0 in the mouse and rat lenses we might expect that the relative contributes of the two water channels to the water permeability of peripheral fiber cells of the outer cortex would be different between the two species.

To test this hypothesis, the water permeability of mouse and rat fiber cells needed to be directly compared. However, because of the terminally-differentiated state of lens fiber cells and their thin and extremely elongated morphology measuring water permeability in fiber cells is difficult. Previous studies (6) (51, 52) have presented measurements of the water permeability of lens fiber cells using fiber-cell–derived membrane vesicles, which are spontaneously formed when fiber cells are isolated from the lens in presence of Ca^{2+} ions. To illustrate this process, a series of DIC images is presented from an isolated cluster of rat lens fiber cells that undergoes cell swelling and subsequent formation of individual vesicles after 30 minutes of incubation in Ca^{2+}-containing isotonic saline (Figure 4A). To test whether the distribution of AQP5 and AQP0 observed in fixed lens sections remains preserved in fiber-cell-derived vesicles, mouse and rat fiber vesicles were labeled with specific *C*-terminal anti-

AQP5 and -AQP0 antibodies. Quantification of labeling distribution between cytoplasmic and membrane-bound AQP0/5 was compromised by collapse of the vesicles following paraformaldehyde fixation, however the labeling distribution qualitatively observed in fiber cell membrane vesicles corresponded with results obtained from rat and mouse lens cryosections. Mouse vesicles showed a predominant membrane localization of AQP5 (Figure 4Bi) although occasionally vesicles with cytoplasmic localization were also identified (Figure 4Bii), while AQP0 labeling was always associated with the membrane (Figure 4Biii&iv). In contrast, the majority of membrane vesicles derived from the rat lens displayed predominant cytoplasmic labeling (Figure 4Ci), with a small number of vesicles displaying some membrane labeling (Figure 4Cii). However, like the mouse AQP0 labeling in fiber cell membrane vesicles derived from the rat lens was found associated with the membrane (Figure 4Ciii&iv). Based on observed differences in the relative abundances, subcellular distributions and relative permeability's of AQP0 and AQP5 water channels, we would predict functional heterogeneity in water permeability in fiber-derived membrane vesicles, and furthermore that species differences may be apparent in the relative contribution of AQP5 conductance to overall water permeability.

Measuring the water permeability of mouse and rat fiber cell membrane vesicles.

Two approaches were used to distinguish between the relative contribution of AQP5 and AQP0 to water permeability of lens differentiating fiber cells. Firstly, we utilized the differential sensitivity of AQP5 and AQP0 to Hg^{2+} (33) as a pharmacological tool to delineate the relative contributes of the two water channels to overall water permeability. Secondly, we exploited the observed species-dependent distribution of AQP5 in the outer cortex of the mouse and rat lenses to make measurements where the Hg^{2+}-sensitive AQP5 contribution would be expected to be lower (cytoplasmic AQP5) or higher (membranous AQP5) for fiber vesicles derived from the rat or mouse, respectively.

To validate the use of mercury as a pharmacological blocker of AQP5, it was first applied to mouse lens epithelial cells, which express the mercury-sensitive aquaporins, AQP1 and AQP5. The average P_{H2O} of mouse epithelial cells ($11.45 \pm 0.6 \times 10^{-3}$ AU, n = 23) was halved ($5.4 \pm 0.3 \times 10^{-3}$ AU, n = 9) after inhibition of APQ1/5 with 300 µM $HgCl_2$ (Figure 5). Relative to epithelial cells, fiber cell membrane vesicles from the mouse had an average P_{H2O} ($7.5 \pm 0.8 \times 10^{-3}$ AU, n = 38), some 32% less than the P_{H2O} of epithelial cells. It was found that P_{H2O} of mouse fiber cell vesicles displayed significant variability. While one third of mouse fibre-derived membrane vesicles gave P_{H2O} values that were similar in magnitude to those measured in mouse lens epithelia, a second population showed a lower water permeability that was some 73% lower than the P_{H2O} of epithelial cells, a result that was similar to what had previously been reported in the literature (50, 51). Pre-incubated mouse fiber-derived membrane vesicles exposed to Hg^{2+} significantly reduced the observed average P_{H2O} ($4.6 \pm 0.6 \times 10^{-3}$ AU, n = 19, $P < 0.02$) and eliminated the sub-group of vesicles with higher P_{H2O} values seen in the absence of mercury (Figure 5).

The same functional dissection of mercury-sensitive water permeability was performed on rat lenses (Figure 6). As seen in the mouse, rat epithelial cells had a high P_{H2O} ($14.4 \pm 0.9 \times 10^{-3}$ AU, n = 30) that was inhibited ($6.8 \pm 0.9 \times 10^{-3}$ AU, n = 19) in presence of mercury (Figure 6). The average P_{H2O} of rat fiber-derived membrane vesicles ($4.8 \pm 0.6 \times 10^{-3}$ AU, n = 30), was ~3-fold lower than the water permeability measured in rat lens epithelial cells. However, unlike the mouse, rat fiber-derived membrane vesicles consisted of one large group of vesicles exhibiting this low P_{H2O}, with only 5 vesicles out of 30 that exhibited higher P_{H2O} values that mirrored those seen in rat epithelial cells. Incubation with Hg^{2+} of rat fiber-derived membrane vesicles showed a small, but not significant, reduction in P_{H2O} ($3.9 \pm 0.4 \times 10^{-3}$AU, n = 15) and the absence of the sub-group of vesicles which exhibited higher P_{H2O} values. In summary, the comparative mercury sensitivities of mouse and rat fiber-derived membrane

vesicles seem to be consistent with their immunohistochemical localizations within both fixed lens sections (Figure 2&3) and membrane vesicles (Figure 4). Taken together, it appears that AQP5 is present in the membrane and contributes, along with AQP0, to the overall water permeability of fiber cells in the outer cortex of the mouse lens. In the rat lens, where AQP5 exists predominately as a pool of cytoplasmic water channels, AQP5 does not appear to make a significant contribution to overall water permeability of cortical fiber cells, as evidenced by the Hg^{2+}-insensitivity of the P_{H2O} measured in rat fiber cell membrane vesicles. This suggests that in the outer cortex of the rat lens that AQP0 mediates water permeability.

Membrane insertion of AQP5 increases the mercury-sensitive water permeability of rat fiber-derived membrane vesicles

In other tissues, AQP5 has been shown to be a regulated water channel which, in response to osmotic challenge, increases water permeability through translocation to the plasma membrane (26, 27, 58). We therefore investigated whether the process of organ culturing lenses under conditions of osmotic challenge could also induce an insertion of AQP5 into the membranes of fiber cells in the outer cortex of the lens (Figure 7), and whether such an insertion would subsequently increase the mercury-sensitive water permeability of fiber cell membrane vesicles isolated from organ cultured lenses (Figure 8). Interestingly, we found that simply organ-culturing lenses in isotonic AAH was sufficient to induce an increase in the membrane localization of AQP5 in both the mouse (Figure 7B-E) and rat (Figure 7F-I) lenses, relative to what was observed when lenses were fixed immediately following removal from the eye. Incubating mouse lenses for two hours in isotonic AAH induced translocation of AQP5 to the membranes of superficial fiber cells in the localized bow region of the outer cortex (Figure 7C) in comparison to immediately fixed lenses where AQP5 was only cytoplasmic (Figure 7B). There was no additional change in the localization of AQP5 in the

deeper regions of the outer cortex where AQP5 remained membranous in lenses that were fixed immediately upon removal from the eye (Figure 7D) and organ cultured mouse lenses (Figure 7E). As previously described, the subcellular distribution of AQP5 labeling in immediately-fixed rat lenses was predominantly cytoplasmic throughout the outer cortex (Figure 7F&H). However, an overnight incubation of rat lenses in isotonic AAH resulted in a switch in AQP5 localization into the membrane in peripheral differentiating fiber cells (Figure 7G), with this membrane localization becoming even more prominent in fiber cells located in the deeper regions of the outer cortical region (Figure 7I). While we do not yet understand the signaling mechanisms responsible for this apparent insertion of AQP5 from a cytoplasmic pool into the membrane, we can use the observed phenomenon to investigate whether this increased membrane insertion of AQP5 alters the mercury-sensitive fraction of the water permeability measured in fiber-derived membrane vesicles. Unfortunately, it is technically challenging to derive fiber cell vesicles from the small (~1-5% of total outer cortex area) superficial outer cortical region of the mouse lens that exhibits membrane insertion of AQP5 in response to organ culture. Hence, measurements of water permeability post-organ culture were only performed on rat fiber-derived vesicles where the biggest increase in Hg^{2+}-sensitive P_{H2O} would be expected to be observed following organ culture.

Fiber-derived membrane vesicles were therefore prepared from the outer cortex of organ-cultured rat lenses, and their water permeability tested using the fluorescence-based functional assay for water permeability (Figure 8). We found that in comparison to native rat vesicles (P_{H2O} = 4.8 ± 0.6 x 10^{-3} AU, n = 30), vesicles derived from organ-cultured rat lenses had a significantly higher average P_{H2O} (7.2 ± 0.6 x 10^{-3} AU, n=31, P < 0.01). The observed increase in average P_{H2O} appeared to be due to AQP5 insertion, since the addition of Hg^{2+} to vesicles prepared from organ cultured lenses produced a significant reduction in P_{H2O} (4.2 ±

1 0.6 x 10^{-3} AU, n = 18, P < 0.015) to values that were found to be not significantly different to
2 the average P_{H2O} measured in acutely-isolated lenses, where AQP5 was predominantly
3 located in the cytoplasm of peripheral fiber cells. These results suggest that in the rat lens
4 AQP5 can be dynamically recruited to the membranes of differentiating fiber cells to increase
5 water permeability in the outer cortex of the lens.

6

7 **DISCUSSION**

8 In this study we have extended our previous observations (20) of species differences in the
9 subcellular location of AQP5 in mouse and rat lenses, and in addition have shown that AQP5
10 contributes to the water permeability of fiber cell membranes. Furthermore, we have shown
11 that this contribution of AQP5 to overall water permeability can be increased by the
12 trafficking of AQP5 from a cytoplasmic pool to the fiber cell membrane. In both rat and
13 mouse lenses, AQP5 could be found in distinct cytoplasmic or membranous pools in the outer
14 cortex, but the extent of cytoplasmic AQP5 labeling was more extensive in the rat than the
15 mouse lens (Figures 2 &3). In contrast, AQP0, was always found to be associated with the
16 membranes of cortical fiber cells in both species (Figure 3&4). These species-specific
17 differences in the subcellular distribution of AQP5 appeared to be maintained in the fiber cell
18 membrane vesicles isolated from the outer cortex of the mouse and rat lens (Figure 4). From
19 this observation, we expected that the functional measurements of P_{H2O} in the vesicles
20 isolated from the mouse and rat lens would exhibit heterogeneity in P_{H2O} values that reflect
21 the differences in the subcellular location of AQP5, the higher protein abundance of AQP0
22 relative to AQP5, and the higher P_{H2O} of water channels formed from AQP5 relative to
23 AQP0.

Consistent with previous reports (50), measured P_{H2O} in epithelial cells isolated from mouse (Figure 5) and rat (Figure 6) lenses were both significantly inhibited by Hg^{2+}, and were higher than the measured P_{H2O} of fiber-derived membrane vesicles. However, the current study revealed significant Hg^{2+}-sensitive water permeability in fiber-derived membrane vesicles isolated from the mouse lens (Figure 5). The observed range of P_{H2O} values recorded in this study tends to mirror the heterogeneity in membrane vs cytoplasmic labeling of AQP5 and membrane labelling of AQP0 observed immunohistochemically in both lens sections, and in vesicles isolated from cortical fiber cells of the mouse lens. Since a subset of mouse fiber cell membrane vesicles displayed P_{H2O} values equivalent to those observed in the morphologically distinct epithelial cells (Figure 1A) and this subset of high vesicles with high P_{H2O} was eliminated in the presence of Hg^{2+}, we can conclude that these vesicles contain in addition to AQP0, the Hg^{2+}-sensitive water channels AQP1/5. Furthermore, since AQP1 expression has been shown to be restricted to the lens epithelium (46) we can assume that the high P_{H2O} permeability observed in this subset of mouse vesicles is mediated by presence of AQP5 in the membranes of these vesicles. The remaining vesicles exhibited a lower, Hg^{2+}-insensitive P_{H2O}, which we attribute to the sole presence of AQP0 water channels in these particular vesicles. Thus relative to an earlier study that analyzed P_{H2O} in the mouse lens using a small number of vesicles (51), the larger sample size of our current study provides a more accurate representation of the heterogeneity in abundance and membrane distribution of AQP0 and AQP5 now known to exist in the mouse lens. Our measurements appear to confirm that, in the mouse lens, AQP5 forms a functional water channel which in combination with AQP0, makes a significant contribution to the water permeability of fiber cells in the outer cortex.

In the rat lens, immunolabeling in lens sections (Figure 2 and 3) and fiber cell membrane vesicles (Figure 4) showed that AQP5 was predominantly localized in the cytoplasm.

Functional measurement of P_{H2O} were consistent with this cytoplasmic location of AQP5, since P_{H2O} measurements in rat fiber cell membrane vesicles were dominated by a lower Hg^{2+}-insensitive basal $P_{H2O,}$ which can be assigned to AQP0 (Figure 6). Interestingly, the magnitude of Hg^{2+}-sensitive water permeability measured in rat fiber-derived membrane vesicles was altered by organ culturing rat lenses in isotonic AAH overnight, and this could be correlated with insertion of AQP5 into cortical fiber cell membranes (Figure 7). AQP5 insertion increased the mean P_{H2O} values, which were subsequently shown to be sensitive to Hg^{2+} (Figure 8). Taken together, our localization and functional studies in lenses of two rodent species demonstrate that AQP5 located in the membrane contributes a Hg^{2+}-sensitive component to the water permeability of cortical fiber cells, that is additional to the basal contribution of AQP0 to P_{H2O}. Furthermore, we show that AQP5 exists in the rat lens as a cytoplasmic pool of water channels, which can be dynamically recruited to increase the P_{H2O} of fiber cell membranes in the outer cortex of the lens.

These conclusions raise two questions that deserve further discussion. Firstly, the observation that organ culture of lenses can stimulate the dynamic insertion of AQP5 into the membranes of differentiating fiber cells in both the mouse and rat lens (Figure 7), raises questions over the pathways that regulate AQP5 membrane insertion in the lens. In other tissues, AQP5 has been found to insert into the apical plasma following phosphorylation of the channel through the cAMP-dependent PKA pathway (58). In addition, exposure to hypertonic challenge was shown to upregulate AQP5 protein expression through an Extracellular signal-Regulated Kinase (ERK) dependent pathway in mouse lung epithelial (MLE-15) cells (22). Together, these studies suggest that phosphorylation of AQP5 might be an important molecular mechanism regulating AQP5 membrane insertion. Although phosphorylated AQP5 has been reported in the mouse lens (34), only one of the two predicted phosphorylation sites of AQP5 (Serine 156, Threonine 259) has been detected in lens tissue (53). Further investigation is

required to establish the phosphorylation status of cytoplasmic and membranous pools of AQP5, in order to understand the mechanisms that control the dynamic insertion of AQP5 in specific regions of the lens.

Secondly, our demonstration that membrane insertion of AQP5 into the differentiating fiber cell membranes increases P_{H2O} does not address the physiological requirement for the lens to dynamically modulate P_{H2O} in the outer cortex. It is interesting to speculate that modulation of P_{H2O} may be required to maintain the gradient in hydrostatic pressure that has been measured in all lenses studied to date (13). This hydrostatic pressure gradient is generated by the flow of water through gap junction channels and ranges from 0 mmHg in the periphery to 335 mmHg in the lens center (14). The pressure gradient is thought to drive intracellular flow of fluid from the lens core to the periphery and is remarkably preserved in lenses from several different species (13). This conservation of the pressure gradient amongst species has led to the suggestion that the gradient is actively modulated to control the water content in the lens core thereby setting the water/protein ratio which, in turn, determines the gradient of refractive index that contributes to the optical properties of the lens (13). Recently, Gao *et al*. demonstrated a link between activation of TRP channels, the alteration in Na/K ATPase activity, and the modulation of hydrostatic pressure in the mouse lens (15). Intriguingly, recent reports have revealed a synergistic association between the mechano-sensitive TRPV4 and aquaporin water channels to affect changes in fluid transportation to preserve cell volume (37), (29),(12). As a working hypothesis it is intriguing to speculate that the dynamic regulation of AQP5 membrane trafficking alters the water permeability of outer cortical fiber cells to modulate the hydrostatic pressure gradient and thereby maintain the optical properties of the lens. Testing this hypothesis will be the focus of future work.

ACKNOWLEDGEMENTS

Mrs. Petrova was the recipient of a University of Auckland Doctoral Scholarship. The authors acknowledge the support of NIH (Grant #EY13462) and a RAEng/EPSRC Postdoctoral Fellowship to Dr. Webb.

REFERENCES

1. **Agre P, King LS, Yasui M, Guggino WB, Ottersen OP, Fujiyoshi Y, Engel A, and Nielsen S**. Aquaporin water channels--from atomic structure to clinical medicine. *The Journal of physiology* 542: 3-16, 2002.
2. **Agre P, Preston GM, Smith BL, Jung JS, Raina S, Moon C, Guggino WB, and Nielsen S**. Aquaporin CHIP: the archetypal molecular water channel. *American Journal of Physiology-Renal Physiology* 265: F463-F476, 1993.
3. **Ball LE, Garland DL, Crouch RK, and Schey KL**. Post-translational modifications of aquaporin 0 (AQP0) in the normal human lens: spatial and temporal occurrence. *Biochemistry* 43: 9856-9865, 2004.
4. **Bassnett S, Shi Y, and Vrensen GFJM**. Biological glass: structural determinants of eye lens transparency. *Philosophical Transactions of the Royal Society of London B: Biological Sciences* 366: 1250-1264, 2011.
5. **Bassnett S, Wilmarth PA, and David LL**. The membrane proteome of the mouse lens fiber cell. *Molecular Vision* 15: 2448-2463, 2009.
6. **Bhatnagar A, Ansari NH, Wang L, Khanna P, Wang C, and Srivastava SK**. Calcium-mediated disintegrative globulization of isolated ocular lens fibers mimics cataractogenesis. *Experimental Eye Research* 61: 303-310, 1995.
7. **Bok D, Dockstader J, and Horwitz J**. Immunocytochemical localization of the lens main intrinsic polypeptide (MIP26) in communicating junctions. *The Journal of Cell Biology* 92: 213-220, 1982.
8. **Bondy C, Chin E, Smith BL, Preston GM, and Agre P**. Developmental gene expression and tissue distribution of the CHIP28 water-channel protein. *Proceedings of the National Academy of Sciences* 90: 4500-4504, 1993.
9. **Borgnia M, Nielsen S, Engel A, and Agre P**. Cellular and molecular biology of the aquaporin water channels. *Annual Review of Biochemistry* 68: 425-458, 1999.
10. **Chandy G, Zampighi GA, Kreman M, and Hall JE**. Comparison of the water transporting properties of MIP and AQP1. *The Journal of Membrane Biology* 159: 29-39, 1997.
11. **Farjo R, Peterson WM, and Naash MI**. Expression profiling after retinal detachment and reattachment: a possible role for aquaporin-0. *Investigative ophthalmology & visual science* 49: 511-521, 2008.
12. **Galizia L, Pizzoni A, Fernandez J, Rivarola V, Capurro C, and Ford P**. Functional interaction between AQP2 and TRPV4 in renal cells. *Journal of Cellular Biochemistry* 113: 580-589, 2012.
13. **Gao J, Sun X, Moore LC, Brink PR, White TW, and Mathias RT**. The effect of size and species on lens intracellular hydrostatic pressure. *Investigative Ophthalmology & Visual Science* 54: 183, 2013.
14. **Gao J, Sun X, Moore LC, White TW, Brink PR, and Mathias RT**. Lens intracellular hydrostatic pressure is generated by the circulation of sodium and modulated by gap junction coupling. *The Journal of General Physiology* 137: 507-520, 2011.
15. **Gao J, Sun X, White TW, Delamere NA, and Mathias RT**. Feedback Regulation of Intracellular Hydrostatic Pressure in Surface Cells of the Lens. *Biophysical Journal* 109: 1830-1839, 2015.
16. **Gold MG, Reichow SL, O'Neill SE, Weisbrod CR, Langeberg LK, Bruce JE, Gonen T, and Scott JD**. AKAP2 anchors PKA with aquaporin-0 to support ocular lens transparency. *EMBO molecular medicine* 4: 15-26, 2012.
17. **Gonen T, Cheng Y, Sliz P, Hiroaki Y, Fujiyoshi Y, Harrison SC, and Walz T**. Lipid-protein interactions in double-layered two-dimensional AQP0 crystals. *Nature* 438: 633-638, 2005.
18. **Gonen T, Sliz P, Kistler J, Cheng Y, and Walz T**. Aquaporin-0 membrane junctions reveal the structure of a closed water pore. *Nature* 429: 193-197, 2004.

19. **Grey AC, Li L, Jacobs MD, Schey KL, and Donaldson PJ**. Differentiation-dependent modification and subcellular distribution of aquaporin-0 suggests multiple functional roles in the rat lens. *Differentiation* 77: 70-83, 2009.
20. **Grey AC, Walker KL, Petrova RS, Han J, Wilmarth PA, David LL, Donaldson PJ, and Schey KL**. Verification and spatial localization of aquaporin-5 in the ocular lens. *Experimental Eye Research* 108: 94-102, 2013.
21. **Harries WE, Akhavan D, Miercke LJ, Khademi S, and Stroud RM**. The channel architecture of aquaporin 0 at a 2.2-Å resolution. *Proceedings of the National Academy of Sciences of the United States of America* 101: 14045-14050, 2004.
22. **Hoffert JD, Leitch V, Agre P, and King LS**. Hypertonic induction of aquaporin-5 expression through an ERK-dependent pathway. *Journal of Biological Chemistry* 275: 9070-9077, 2000.
23. **Iandiev I, Pannicke T, Härtig W, Grosche J, Wiedemann P, Reichenbach A, and Bringmann A**. Localization of aquaporin-0 immunoreactivity in the rat retina. *Neuroscience letters* 426: 81-86, 2007.
24. **Iandiev I, Pannicke T, Reichel MB, Wiedemann P, Reichenbach A, and Bringmann A**. Expression of aquaporin-1 immunoreactivity by photoreceptor cells in the mouse retina. *Neuroscience letters* 388: 96-99, 2005.
25. **Ishibashi K, Hara S, and Kondo S**. Aquaporin water channels in mammals. *Clinical and experimental nephrology* 13: 107-117, 2009.
26. **Ishikawa Y, Eguchi T, Skowronski MT, and Ishida H**. Acetylcholine acts on M 3 muscarinic receptors and induces the translocation of aquaporin5 water channel via cytosolic Ca 2+ elevation in rat parotid glands. *Biochemical and biophysical research communications* 245: 835-840, 1998.
27. **Ishikawa Y, Skowronski MT, Inoue N, and Ishida H**. α 1-Adrenoceptor-induced trafficking of aquaporin-5 to the apical plasma membrane of rat parotid cells. *Biochemical and biophysical research communications* 265: 94-100, 1999.
28. **Jacobs MD, Donaldson PJ, Cannell MB, and Soeller C**. Resolving morphology and antibody labeling over large distances in tissue sections. *Microscopy Research and Technique* 62: 83-91, 2003.
29. **Jo AO, Ryskamp DA, Phuong TTT, Verkman AS, Yarishkin O, MacAulay N, and Križaj D**. TRPV4 and AQP4 Channels Synergistically Regulate Cell Volume and Calcium Homeostasis in Retinal Müller Glia. *The Journal of Neuroscience* 35: 13525-13537, 2015.
30. **Kierdaszuk B**. From discrete multi-exponential model to lifetime distribution model and power law fluorescence decay function. *Journal of Spectroscopy* 24: 399-407, 2010.
31. **Kim I-B, Oh S-J, Nielsen S, and Chun M-H**. Immunocytochemical localization of aquaporin 1 in the rat retina. *Neuroscience letters* 244: 52-54, 1998.
32. **King LS, Kozono D, and Agre P**. From structure to disease: the evolving tale of aquaporin biology. *Nature Reviews Molecular Cell Biology* 5: 687-698, 2004.
33. **Krane CM, Melvin JE, Nguyen HV, Richardson L, Towne JE, Doetschman T, and Menon AG**. Salivary acinar cells from aquaporin 5-deficient mice have decreased membrane water permeability and altered cell volume regulation. *Journal of Biological Chemistry* 276: 23413, 2001.
34. **Kumari SS, Varadaraj M, Yerramilli VS, Menon AG, and Varadaraj K**. Spatial expression of aquaporin 5 in mammalian cornea and lens, and regulation of its localization by phosphokinase A. *Molecular Vision* 18: 957, 2012.
35. **Ladokhin AS, and White SH**. Alphas and taus of tryptophan fluorescence in membranes. *Biophysical journal* 81: 1825-1827, 2001.
36. **Lakowicz JR**. On Spectral Relaxation in Proteins. *Photochemistry and photobiology* 72: 421-437, 2000.
37. **Liu X, Bandyopadhyay B, Nakamoto T, Singh B, Liedtke W, Melvin JE, and Ambudkar I**. A Role for AQP5 in Activation of TRPV4 by Hypotonicity: concerted involvement of AQP5 and TRPV4 in regulation of cell volume recovery. *Journal of Biological Chemistry* 281: 15485-15495, 2006.

38. **Lovicu FJ, McAvoy JW, and De Iongh RU**. Understanding the role of growth factors in embryonic development: insights from the lens. *Philosophical Transactions of the Royal Society B: Biological Sciences* 366: 1204-1218, 2011.
39. **Mathias RT, Kistler J, and Donaldson P**. The lens circulation. *Journal of Membrane Biology* 216: 1-16, 2007.
40. **Mathias RT, Rae JL, and Baldo GJ**. Physiological properties of the normal lens. *Physiological Reviews* 77: 21-50, 1997.
41. **McAvoy JW, Chamberlain CG, de Iongh RU, Hales AM, and Lovicu FJ**. Lens development. *Eye* 13 (Pt 3b): 425-437, 1999.
42. **Mulders SM, Preston GM, Deen PM, Guggino WB, van Os CH, and Agre P**. Water channel properties of major intrinsic protein of lens. *Journal of Biological Chemistry* 270: 9010-9016, 1995.
43. **Patil RV, Saito I, Yang X, and Wax MB**. Expression of Aquaporins in the Rat Ocular Tissue. *Experimental Eye Research* 64: 203-209, 1997.
44. **Petrova RS, Schey KL, Donaldson PJ, and Grey AC**. Spatial distributions of AQP5 and AQP0 in embryonic and postnatal mouse lens development. *Experimental Eye Research* 132: 124-135, 2015.
45. **Rose KM, Wang Z, Magrath GN, Hazard ES, Hildebrandt JD, and Schey KL**. Aquaporin 0-calmodulin interaction and the effect of aquaporin 0 phosphorylation. *Biochemistry* 47: 339-347, 2008.
46. **Ruiz-Ederra J, and Verkman AS**. Accelerated cataract formation and reduced lens epithelial water permeability in aquaporin-1-deficient mice. *Investigative ophthalmology & visual science* 47: 3960-3967, 2006.
47. **Savage DF, and Stroud RM**. Structural Basis of Aquaporin Inhibition by Mercury. *Journal of Molecular Biology* 368: 607-617, 2007.
48. **Varadaraj K, Kumari S, Shiels A, and Mathias RT**. Regulation of aquaporin water permeability in the lens. *Investigative Ophthalmology & Visual Science* 46: 1393-1402, 2005.
49. **Varadaraj K, Kumari SS, and Mathias RT**. Functional Expression of Aquaporins in Embryonic, Postnatal, and Adult Mouse Lenses. *Developmental dynamics : an official publication of the American Association of Anatomists* 236: 1319-1328, 2007.
50. **Varadaraj K, Kumari SS, and Mathias RT**. Functional expression of aquaporins in embryonic, postnatal, and adult mouse lenses. *Developmental Dynamics* 236: 1319-1328, 2007.
51. **Varadaraj K, Kushmerick C, Baldo GJ, Bassnett S, Shiels A, and Mathias RT**. The role of MIP in lens fiber cell membrane transport. *The Journal of Membrane Biology* 170: 191-203, 1999.
52. **Wang L, Bhatnagar A, Ansari NH, Dhir P, and Srivastava SK**. Mechanism of calcium-induced disintegrative globulization of rat lens fiber cells. *Investigative Ophthalmology & Visual Science* 37: 915-922, 1996.
53. **Wang Z, Han J, David LL, and Schey KL**. Proteomics and Phosphoproteomics Analysis of Human Lens Fiber Cell MembranesAnalysis of Human Lens Fiber Cell Membranes. *Investigative ophthalmology & visual science* 54: 1135-1143, 2013.
54. **Wang Z, Han J, and Schey KL**. Spatial differences in an integral membrane proteome detected in laser capture microdissected samples. *Journal of Proteome Research* 7: 2696-2702, 2008.
55. **Wistow G, Bernstein SL, Wyatt MK, Behal A, Touchman JW, Bouffard G, Smith D, and Peterson K**. Expressed sequence tag analysis of adult human lens for the NEIBank Project: over 2000 non-redundant transcripts, novel genes and splice variants. *Molecular Vision* 8: 171-184, 2002.
56. **Włodarczyk J, and Kierdaszuk B**. Interpretation of fluorescence decays using a power-like model. *Biophysical journal* 85: 589-598, 2003.
57. **Yang B, and Verkman AS**. Water and glycerol permeabilities of aquaporins 1-5 and MIP determined quantitatively by expression of epitope-tagged constructs in Xenopus oocytes. *Journal of Biological Chemistry* 272: 16140-16146, 1997.
58. **Yang F, Kawedia JD, and Menon AG**. Cyclic AMP regulates aquaporin 5 expression at both transcriptional and post-transcriptional levels through a protein kinase A pathway. *Journal of Biological Chemistry* 278: 32173-32180, 2003.

1

FIGURE LEGENDS

Figure 1: Fluorescent assay used to calculate the rate of change in cell/vesicle volume. (A) Representative images of a single rat epithelial cell (*top panel*) and fiber cell membrane vesicle (*bottom panel*) loaded with calcein, before and after exposure to hypertonic (390 $mOsmL^{-1}$) saline. A single DIC image was taken prior to the exposure to hypertonic saline, and subsequently used to calculate the initial area of the epithelial cell or membrane vesicle and also to differentiate between epithelial cells and vesicles by the presence or absence of a cell nucleus. Representative images from the initial exposure to isotonic (25 s), hypertonic (75 s) and back to isotonic (145 s) saline are shown. (B) Representative bleach-corrected time course, showing the normalized change in calcein fluorescence intensity in response to a hypertonic challenge. Fluorescence intensity was collected from a central region of interest within individual vesicles. (C) The initial change in fluorescence intensity of two vesicles in response to hypertonic challenge, in either the absence and presence of mercury, fitted with monoexponential equations to extract the rate of change in cell volume (τ), used to calculate the water permeability (P_{H2O}, Equation 2). Scale bar 5 μm.

Figure 2: Comparison of the subcellular localization of AQP5 in axial sections taken from mouse and rat lenses. (A) A low-power overview of an axial mouse lens section, labeled with the general membrane marker WGA (red) and the nuclear stain DAPI (blue) to define three regions where the subcellular location of AQP5 (green) is subsequently compared between mouse (B) and rat (C). (B) Higher magnification images from the mouse lens reveal cytoplasmic labeling of AQP5 which is restricted to a narrow and superficial region localized around the equator, designated by the dotted line (Region 1B). Beyond this region AQP5 was found to be associated with the membrane at both the anterior (Region 2B) and posterior (Region 3B) poles of the lens. (C) Higher magnification images from the rat

lens showed that AQP5 labeling remained cytoplasmic in the equator (Region 1C), in the anterior (Region 2C) and posterior (Region 3C) poles of the lens. For clarity of display a mirror image, in which WGA labeling is omitted, is presented on the right hand side next to each double- or triple-labeled image.

Figure 3: Comparison of the membrane localization of AQP0 and AQP5 in the outer cortex of the mouse and rat lenses. (A) An equatorial section of rat lens labeled with the membrane marker WGA (red) and the nuclear stain DAPI (blue) showing the regions (white boxes) from which high magnification images of the subcellular location of AQP0 and AQP5 were obtained from the mouse (B-E) and rat (F-I) lens. To account for the differences of the sizes of the mouse and rat lenses, labeling for AQP0 and AQP5 was obtained from equivalent regions represented with an r/a ratio - where at r/a=1 indicates a region adjacent to the capsule and r/a=0 corresponds to the lens core. For both the mouse and rat lenses r/a=0.98 for the region next to the capsule (B, C, F and G). In the deeper outer cortical region r/a=0.90 for the mouse lens (D, E) and r/a=0.77 for the rat lens (H, I). In the mouse (B) and rat (F) lens, AQP0 (green) is expressed around the entire membrane of differentiating fiber cells localized adjacent to the capsule while AQP5 (green), in the same region, in both the mouse (C) and rat (G) lenses, was localized only in the cytoplasm. In deeper regions of the outer cortex in both the mouse (D) and rat (H) lenses AQP0 continued to be membranous. In the same region changes in the expression of AQP5 were observed since in the mouse lens (E) AQP5 labeling (green) was translocated exclusively to the membranes of differentiating fiber cells while in the rat lenses (I) AQP5 labeling continued to be strongly cytoplasmic. n, nuclei; blue, DAPI.

Figure 4: The subcellular distribution of AQP0 and AQP5 in membrane vesicles formed from fiber cells isolated from the mouse or rat lens. (A) A clump of fiber cells isolated from the rat lens undergoes a process of vesiculation to spontaneously form a cluster of membrane vesicles after 30 minutes of incubation in the presence of Ca^{2+}. (B) In membrane vesicles isolated from the mouse lens AQP5 (green) was predominantly associated with the membranes (Bi), but could occasionally be also found in the cytoplasm (Bii). In double labeled vesicles, AQP0 (red) was always membranous and could be found co-expressed with either higher (Biii) or lower levels of AQP5 labeling (Biv). (C) In the rat, AQP5 was predominately cytoplasmic (Ci), although some vesicles exhibited membrane labeling for AQP5 (Cii). In double labeled rat vesicles, AQP0 was always membranous while AQP5 labeling was usually cytoplasmic (Ciii), although vesicles that co-expressed both AQP0 and AQP5 in the membrane were occasionally detected (Civ). Scale bar in A, B and C is 5µm.

Figure 5: Water permeability of epithelial cells and fiber cell membrane vesicles in the mouse lens. Scatter plots showing the water permeability (P_{H2O}) of mouse epithelial cells and fiber cell membrane vesicles in the presence and absence of 300 µM $HgCl_2$. The addition of $HgCl_2$ significantly reduced the P_{H2O} of mouse epithelial cells and fiber cell membrane vesicles. *** ($P < 0.0001$), *($P < 0.02$); (n) number of cells or membrane vesicles; Bars show Mean ± SEM.

Figure 6: Water permeability of epithelial cells and fiber cell membrane vesicles in the mouse lens. Scatter plots showing the water permeability (P_{H2O}) of rat epithelial cells and fiber cell membrane vesicles in the presence and absence of 300 µM $HgCl_2$. The addition of $HgCl_2$ significantly reduced the P_{H2O} of rat epithelial cells but not rat fiber-derived membrane

vesicles. *** ($P < 0.0001$); NS, not significantly different; (n) number of cells or membrane vesicles; Bars show Mean ± SEM

Figure 7: Dynamic insertion of AQP5 in the cell membranes of organ-cultured rat and mouse lenses incubated in isotonic AAH. (A) Low power overview of an equatorial section of a lens labeled with the membrane marker WGA (*red*) showing two regions (*white boxes*) in the outer cortex where high magnification images were obtained from a mouse (B-E) or rat (F-I) lens, fixed either immediately after removal from the eye (B, D, F, H) or after organ culture in AAH (C, E, G, I). In immediately fixed mouse lenses AQP5 labeling was predominately cytoplasmic in the superficial (B) region, but was membraneous in the deeper regions (D) of the outer cortex. In sections taken from mouse lenses organ cultured for 2 hours, AQP5 labeling was found to colocalize with the membranes of differentiating fiber cells in a discrete zone in the lens periphery (C, arrowhead), and retained its membraneous location in deeper (E) regions of the outer cortex. In immediately fixed rat lenses, AQP5 labeling was predominately cytoplasmic in both the superficial (F) and deeper regions (H) of the outer cortex. In contrast, in sections from rat lenses organ cultured for 17 hours, AQP5 labeling was found in discrete punctae, that colocalized with the membranes of differentiating fiber cells in both peripheral (C) and deeper (E) regions of the outer cortex.

Figure 8: Effect of organ culture on the Hg^{2+}-sensitive water permeability of rat fiber cell membrane vesicles. Scatter plots comparing the water permeability (P_{H2O}) of fiber cell membrane vesicles prepared from lenses fixed either immediately after removal from the eye, or after organ culture in AAH for 17 hours. The addition of 300 µM $HgCl_2$ significantly reduced the P_{H2O} of membrane vesicles prepared from organ cultured rat lenses. **($P < 0.01$); *($P < 0.015$); (*n*) number of cells or membrane vesicles; Bars show Mean ± SEM.

Figures

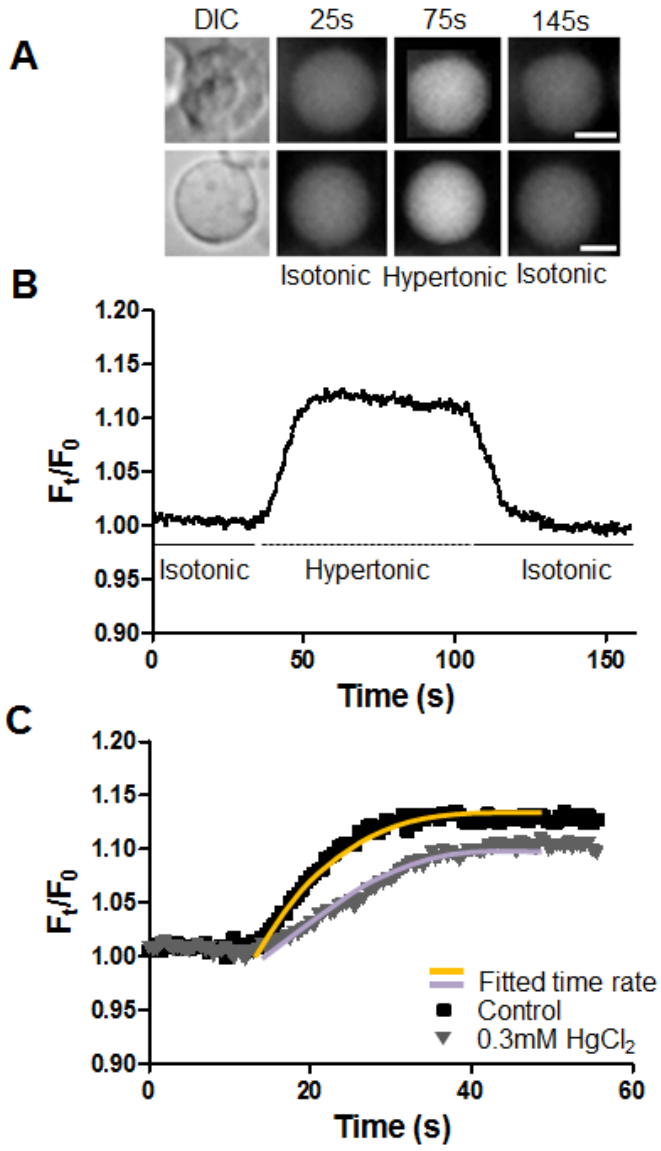

Figure 1.

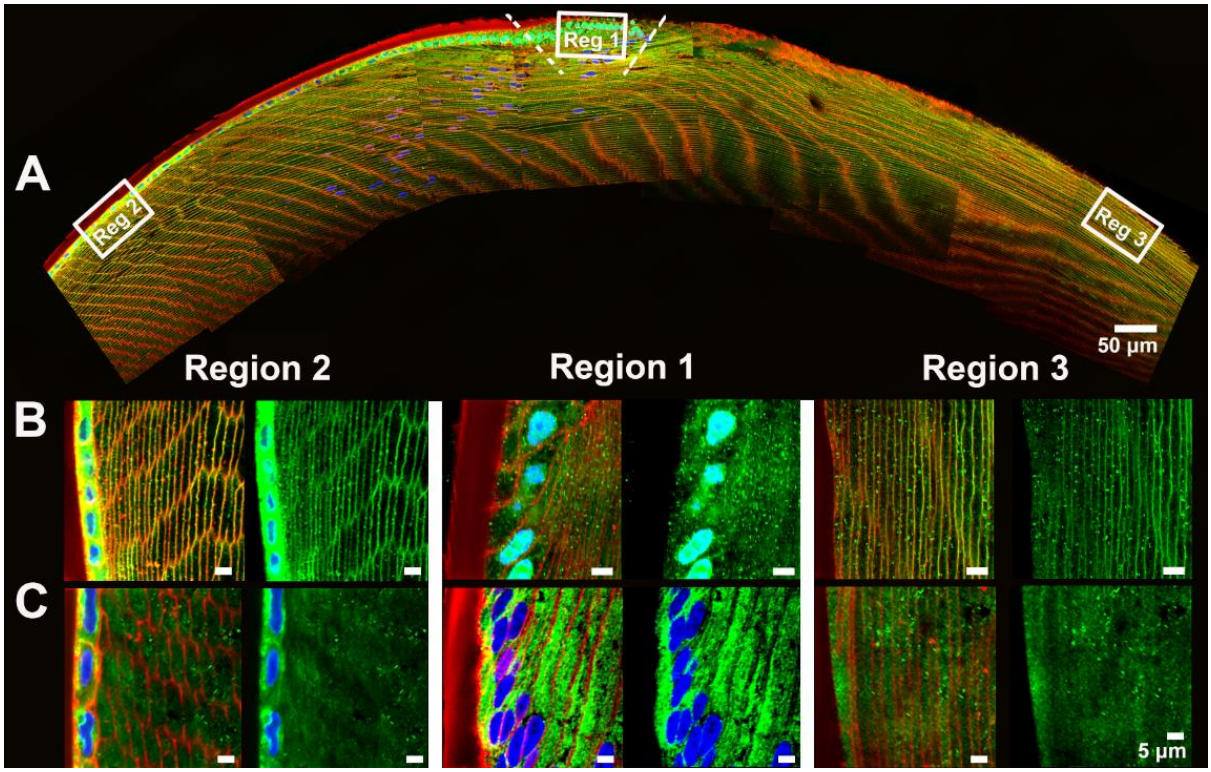

Figure 2.

1

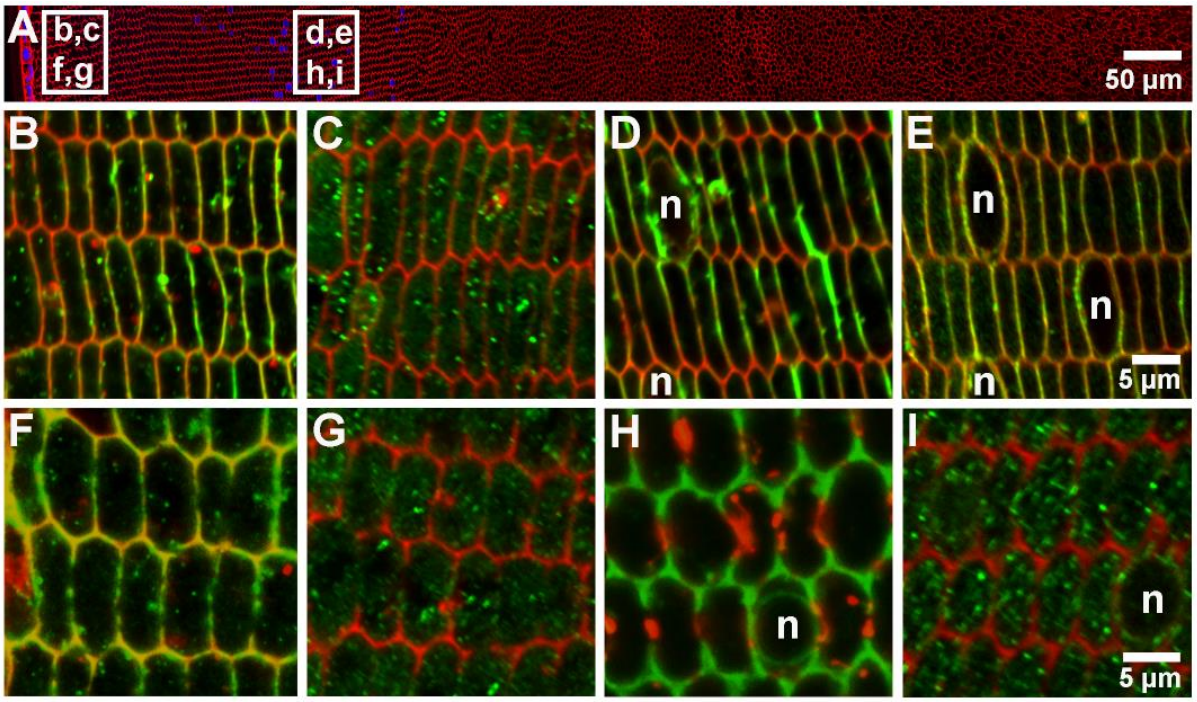

2

3 Figure 3.

1

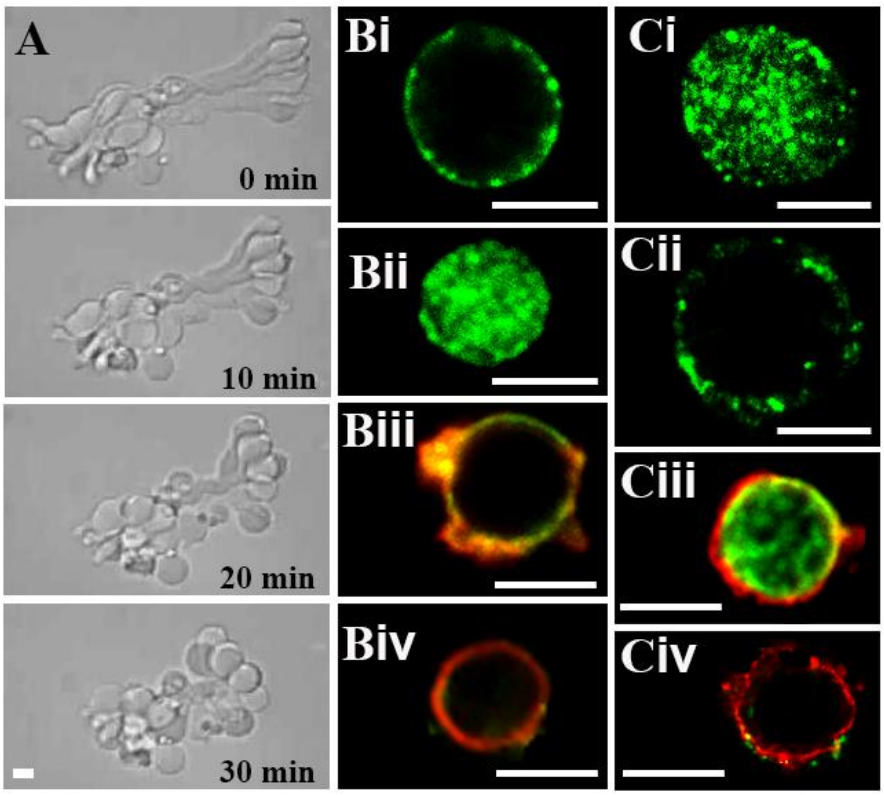

2

3 Figure 4.

4

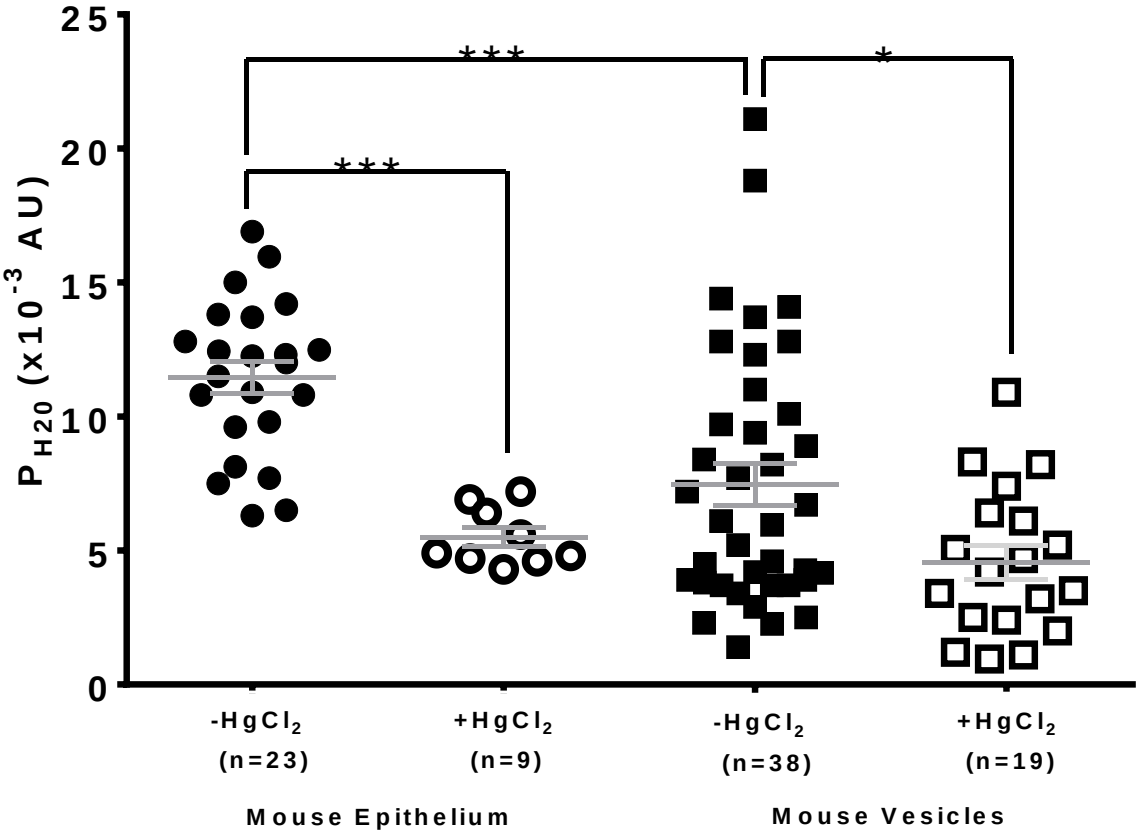
25
20
15
10
5
0
P_{H20} (x10^{-3} AU)
***
***
*
-HgCl$_2$
(n=23)
+HgCl$_2$
(n=9)
-HgCl$_2$
(n=38)
+HgCl$_2$
(n=19)
Mouse Epithelium
Mouse Vesicles

Figure 5.

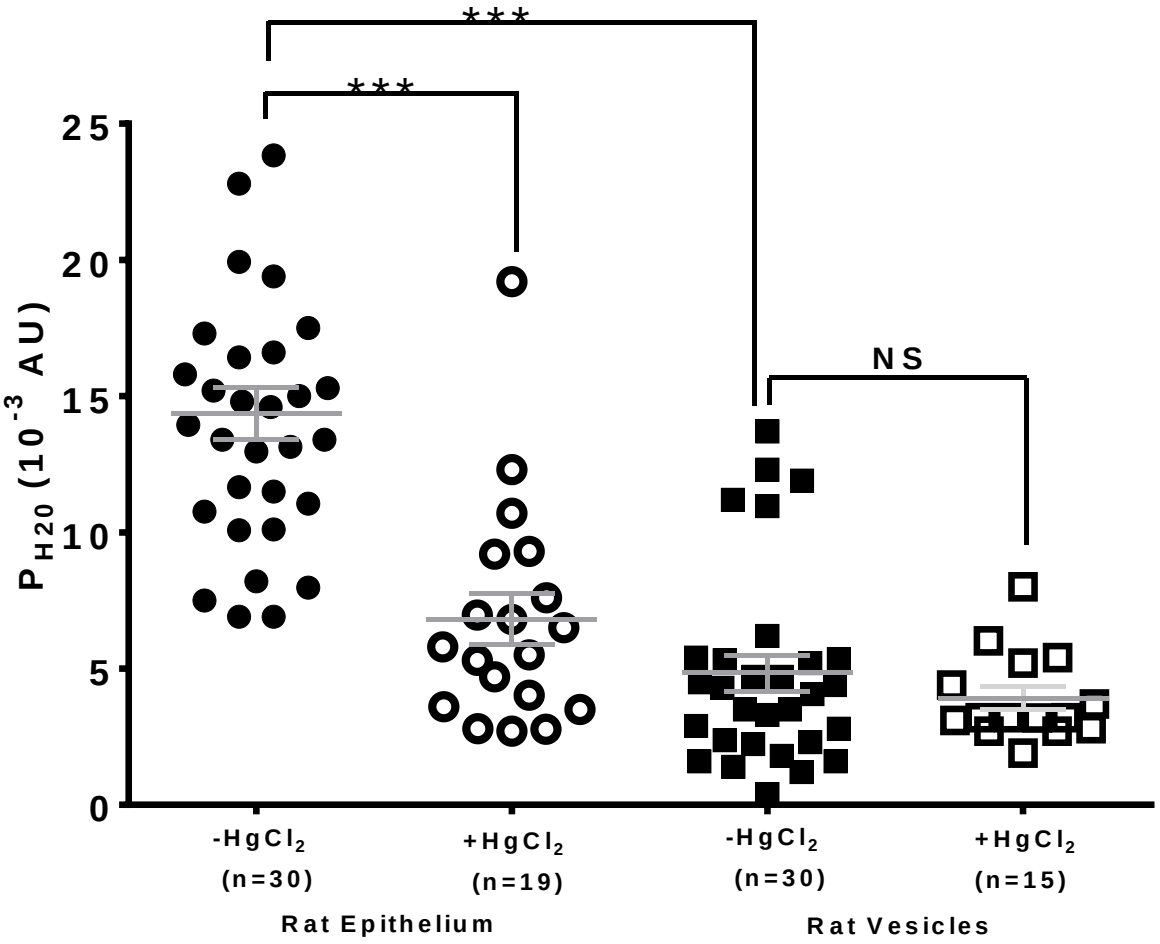
***
***
NS
25
20
15
10
5
0
P_{H20} (10^{-3} AU)
-HgCl2
(n=30)
+HgCl2
(n=19)
-HgCl2
(n=30)
+HgCl2
(n=15)
Rat Epithelium
Rat Vesicles

Figure 6.

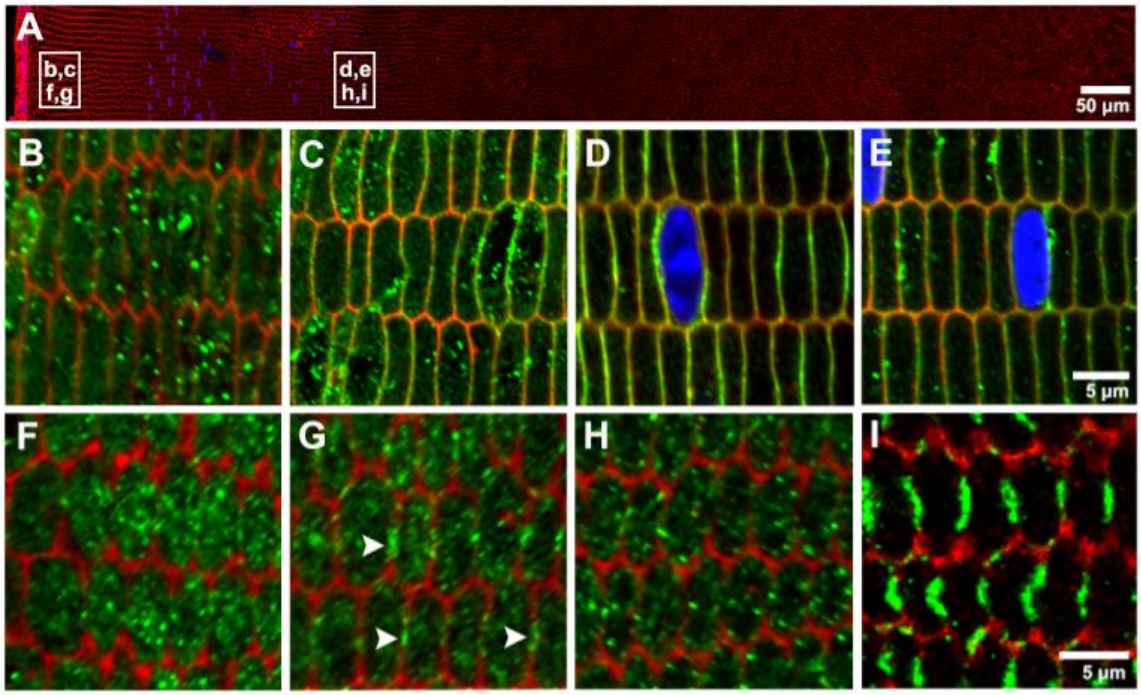

Figure 7.

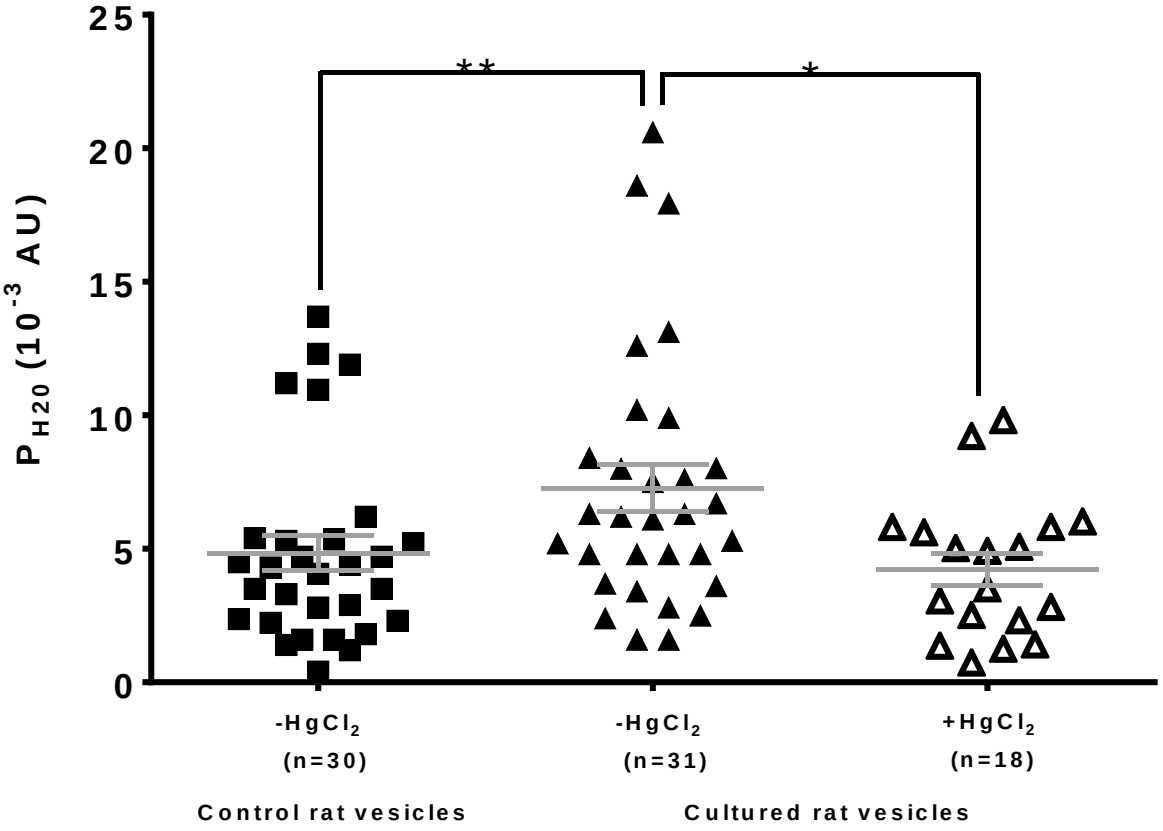
25
20
15
10
5
0
P_{H20} (10^{-3} AU)
**
*
-HgCl2
(n=30)
-HgCl2
(n=31)
+HgCl2
(n=18)
Control rat vesicles
Cultured rat vesicles

Figure 8.